

# IMPLICIT ACTIVE CONTOURS APPLIED TO THE FETAL ECHOCARDIOGRAPHIC IMAGES SEGMENTATION: A COMPARATIVE STUDY.

Santos, J.B<sup>1</sup>, Silva, J.S.<sup>2</sup>, and Antunes<sup>2</sup>, S.G.

<sup>1</sup>*Centro de Engenharia Mecânica, Faculdade de Ciências e Tecnologia, Universidade de Coimbra, Portugal*

<sup>2</sup>*Centro de Instrumentação, Faculdade de Ciências e Tecnologia, Universidade de Coimbra, Portugal*

## Abstract

The goal of this paper deals with the segmentation of medical images, namely cardiac echocardiographic images of newborns to assist the physicians in the identification of several congenital heart defects, like septal defects, valvular malformation, and aorta coarctation. As echographic images are of low quality and very noisy, we propose region based active contour segmentation models. Thus, we compare the usefulness of two methods, namely the piecewise-constant active contour model proposed by Chan and Vese using the Mumford-Shah segmentation model, and the new variational level set formulation proposed by Chunming Li. Important parameters like, shape and size of initial contours, position in the images and propagation direction of the level set will be tested. Also, we evaluate the performance of the two algorithms in terms of: (1) time the contours take to reach the boundaries, in similar conditions; (2) using more than one type of initialization contour, and (3) the effect of image smoothing. Finally, we will present various experimental results using real cardiac echocardiographic images of newborns.

**Keywords:** Active contours, energy minimization, level sets, partial differential equations, segmentation, cardiac echocardiographic images.

## Introduction

Medical imaging, namely echocardiographic imaging, is an important diagnostic tool as it allows the physicians to identify several congenital heart defects. Nowadays, concerning to newborns, several atrial and ventricular defects may be treated through percutaneous closure. Therefore, several echocardiographic parameters should be analysed beforehand in order to determine the feasibility of the procedure. 3D-echo provides a good visualization of the septal defects which enables the operator to easily verify if the patient can support the required closure device without injuring the structures. Also, in the case of valvular malformation 3D echocardiographic images offer intracavitary perspectives of the valves, allowing a detailed analysis of their morphology, as well as coaptation mechanism and valvular regurgitation, if present. These aspects are fundamental to surgical planning. Respecting to aorta coarctation, 3D echocardiography permits endoluminal reconstructions of the coarctation and dynamic measurements of the lesion during the cardiac cycle. Segmentation is often a necessary processing step for three-dimensional (3D) image reconstruction and quantitative analysis. Active contours are among the most successful image segmentation techniques used in several applications, such as computer vision, pattern recognition, and medical image processing. As image segmentation methods, there are two kinds of active contour models according to the force evolving the contours: edge based [1-4] and region-based [5-10].

Edge-based active contours use an edge detector, usually based on the image gradient, to find the boundaries of sub-regions and to attract the contours to the detected boundaries. Most edge based active contour models consist of two parts: the regularity part, which determines the shape of contours, and the edge detection part, which attracts the contour towards the edges. Examples of such models are balloon models [3, 4], geodesic active contours [11, 12], and geometric active contours [2, 13]. These models have as disadvantages, the fact that the active contour relies on the

image gradient operation, edge-based active contours may skip the blurry boundaries, and contours are sensitive to local minima or noise.

Region-based active contours use the statistical information of image intensity within each subset instead of searching geometrical boundaries. Most region-based active contour models consist of two parts: the regularity part, which determines the smooth shape of contours, and the energy minimization part, which searches for uniformity of a desired feature within a subset. An interesting characteristic of region-based active contours is that the initial contours can be located anywhere in the image as region-based segmentation relies on the global energy minimization rather than local energy minimization. Their main advantages over classical explicit active contours [14] are implicit handling of topological changes, numerical stability and independence of parameterisation. However, their main drawback is the additional computational complexity.

In this work we compare the piecewise-constant active contour model proposed by Chan and Vese [5] using the Mumford-Shah segmentation model [7,15], and the new region-based active contour model in a variational level set formulation, proposed by Chunming Li *et al* [16]. In detail, we compare the segmentation quality of the two approaches on real medical images, namely echocardiographic images of newborns. The Chan and Vese model can detect objects with or without strong gradient, automatically detect interior contours, and the initial contour can be placed anywhere in the image. The Chunming Li model draws upon intensity information in local regions at a controllable scale allowing to overcome the difficulties caused by intensity inhomogeneities. Some performance criteria are evaluated to quantify the robustness of the two different active contour models: position, shape, and propagation direction of the initial contour; convergence time for each algorithm; and image smoothing effect.

This paper is organized as follows: in section 2, concepts and mathematics related to both region based active contour models are presented; the results on echocardiographic images are presented in section 3, and finally, the conclusions is formulated in Section 4.

## 2. Active contour models

### 2.1. Piecewise-constant active contour model

Piecewise-constant active contour model was proposed by Chan and Vese using the Mumford-Shah segmentation model. Piecewise-constant active contour model moves deformable contours minimizing an energy function instead of searching edges. A constant approximates the statistical information of image intensity within a subset, and a set of constants, i.e. a piecewise-constant, approximate the statistics of image intensity along the entire domain of an image. The energy function measures the difference between the piecewise-constant and the actual image intensity at every image pixel. The stopping term does not depend on the gradient of the image, as in the classical active contour models, but is instead related to a particular segmentation of the image. The stopping term is based on Mumford-Shah segmentation techniques. In this way, we obtain a model which can detect contours both with and without gradient, for instance objects with very smooth boundaries or even with discontinuous boundaries.

This model consists of the minimization of an energy based-segmentation. Let first explain the basic idea of the model in a simple case. Considering that the image  $u_0$  is formed by two regions of approximately piecewise-constant intensities, of distinct values  $u_0^1$  and  $u_0^0$ . Assume further that the object to be detected is represented by the region with the value  $u_0^1$  and let denote his boundary by  $C_0$ . Then we have  $u_0 \approx u_0^1$  inside the object (inside  $C_0$ ) and  $u_0 \approx u_0^0$  outside the object (outside  $C_0$ ). Now let us consider the following "fitting energy", formed by two terms:

$$F_1(C) + F_2(C) = \int_{inside(C)} |u_0 - c_1|^2 dx dy + \int_{outside(C)} |u_0 - c_2|^2 dx dy, \quad (1)$$

where  $C$  is the auxiliary variable curve, and the constants  $c_1, c_2$ , depending on  $C$ , are the averages of  $u_0$  inside  $C$  and outside  $C$ , respectively. In this case, the boundary of the object is the minimizer of the fitting term,

$$\min_C \{ F_1(C) + F_2(C) \} \approx 0 \approx F_1(C_0) + F_2(C_0). \quad (2)$$

For instance, if the curve  $C$  is outside the object, then  $F_1(C) > 0$  and  $F_2(C) \approx 0$ . If the curve  $C$  is inside the object, then  $F_1(C) \approx 0$  but  $F_2(C) > 0$ . If the curve  $C$  is both inside and outside the object, then  $F_1(C) > 0$  and  $F_2(C) > 0$ . Finally, the fitting energy will be minimized until the  $C = C_0$ , i.e. if the curve  $C$  is on the boundary of the object. Besides the minimization of the fitting term, some regularization terms are added like the length of  $C$  and/or the area inside  $C$ . The energy functional is now,

$$F_1(C) + F_2(C) = \mu \cdot \text{Length}(C) + \nu \cdot \text{Area}(\text{inside}(C)) + \lambda_1 \int_{\text{inside}(C)} |u_0 - c_1|^2 dx dy + \lambda_2 \int_{\text{outside}(C)} |u_0 - c_2|^2 dx dy, \quad (3)$$

where  $\mu > 0, \nu \geq 0, \lambda_1, \lambda_2 > 0$  are fixed parameters.

This active contour model with  $\nu = 0$  and  $\lambda_1 = \lambda_2 = \lambda$  is a particular case of the minimal partition problem of Mumford-Shah [15], in which one looks for the best approximation  $u$  of  $u_0$ , as a function taking only two values, namely

$$\begin{aligned} u &= \text{average}(u_0) \text{ inside } C, \\ u &= \text{average}(u_0) \text{ outside } C; \end{aligned} \quad (4)$$

and with one edge  $C$ , represented by the snake or the active contour.

This particular case of the minimal partition problem can be formulated and solved using the level set method [17].

### 2.1.1. Level-set Formulation

Introducing a level-set function  $\phi$  such that  $C = \{\mathbf{x} \in \Omega : \phi(\mathbf{x}) = 0\}$ . Define the inside and outside of  $C$  by

$$\text{inside}(C) = \{\mathbf{x} \in \Omega : \phi(\mathbf{x}) > 0\}, \text{ and } \text{outside}(C) = \{\mathbf{x} \in \Omega : \phi(\mathbf{x}) < 0\}.$$

Considering the definition of the heaviside function  $H(s)$  to be,

$$H(s) = \begin{cases} 1, & \text{if } s \geq 0 \\ 0, & \text{if } s < 0 \end{cases}$$

and the one-dimensional Dirac delta function  $\delta(s)$  defined by:

$$\delta(s) = \frac{d}{ds} (H(s)),$$

equation (3) can be rewritten as,

$$\begin{aligned}
F(\phi, c_1, c_2) &= \mu \int_{\Omega} |\nabla(\phi)| \delta(\phi) + \nu \int_{\Omega} H(\phi) dx dy \\
&+ \lambda_1 \int_{\Omega} |u_0 - c_1|^2 H(\phi) dx dy + \lambda_2 \int_{\Omega} |u_0 - c_2|^2 (1 - H(\phi)) dx dy
\end{aligned} \tag{5}$$

Having into account that,

$$\text{length}(C) = \int_{\Omega} |\nabla H(\phi(x, y))| dx dy = \int_{\Omega} \delta(\phi(x, y)) \nabla \phi(x, y) dx dy$$

$$\text{area}(\text{inside}(C)) = \int_{\Omega} H(\phi(x, y)) dx dy$$

Keeping  $\phi$  fixed and minimizing the energy  $F(c_1, c_2, \phi)$  with respect to the constants  $c_1$  and  $c_2$ , these can be expressed by

$$c_1 = \frac{\int_{\Omega} u_0(x, y) H(\phi(x, y)) dx dy}{\int_{\Omega} H(\phi(x, y)) dx dy} \tag{6}$$

and

$$c_2 = \frac{\int_{\Omega} u_0(x, y) (1 - H(\phi(x, y))) dx dy}{\int_{\Omega} (1 - H(\phi(x, y))) dx dy} \tag{7}$$

From variational calculus, the minimization of a functional requires the Euler-Lagrange equation to be solved. Note that, in processing with solving the Euler-Lagrange equation, the heaviside and delta functions must be regularized to  $H_{\varepsilon}$  and  $\delta_{\varepsilon}$  so that  $\nabla H_{\varepsilon}(\mathbf{x}) = \delta_{\varepsilon}(\mathbf{x})$ . Thus, the regularized version of the functional (5) becomes,

$$\begin{aligned}
F_{\varepsilon}(\phi, c_1, c_2) &= \mu \int_{\Omega} |\nabla(\phi)| \delta_{\varepsilon}(\phi) + \nu \int_{\Omega} H_{\varepsilon}(\phi) dx dy \\
&+ \lambda_1 \int_{\Omega} |u_0 - c_1|^2 H_{\varepsilon}(\phi) dx dy + \lambda_2 \int_{\Omega} |u_0 - c_2|^2 (1 - H_{\varepsilon}(\phi)) dx dy
\end{aligned} \tag{8}$$

Keeping  $c_1$  and  $c_2$  fixed, and minimizing  $F_{\varepsilon}$  with respect to  $\phi$ , we deduce the associated Euler-Lagrange equation for  $\phi$ :

$$\frac{\partial \phi}{\partial t} = \delta_{\varepsilon}(\phi) \left[ \mu \operatorname{div} \left( \frac{\nabla \phi}{|\nabla \phi|} \right) - \nu - \lambda_1 (u_0 - c_1)^2 + \lambda_2 (u_0 - c_2)^2 \right] = 0, \tag{9}$$

in  $\Omega$  with boundary conditions  $\partial \phi / \partial n = 0$  on  $\partial \Omega$ . The zero level set of  $\phi$  at the steady state is the curve  $C$  which solves the segmentation problem.

## 2.2. Region-based model using intensity information in local regions at a controllable scale.

Chunming Li *et al* [14], have proposed a new region-based active contour model in a variational level set formulation. First, they define a region-scalable fitting (RSF) energy functional in terms of a contour and two fitting functions that locally approximate the image intensities on the two sides of the contour. The optimal fitting functions are shown to be the averages of local intensities on the two sides of the contour. The region-scalability of the RSF energy is due to the kernel function with a scale parameter, which allows the use of intensity information in regions at a controllable scale, from small neighbourhoods to the entire domain. This energy is then incorporated into a variational level set formulation with a level set regularization term.

Let first explain the basic idea of the variational level set formulation. Consider a given vector valued image  $\mathbf{I}: \Omega \rightarrow \mathfrak{R}^n$ , where  $\Omega \subset \mathfrak{R}^n$  is the image domain, and  $n \geq 1$  is the dimension of the vector  $\mathbf{u}(\mathbf{x})$ . In particular,  $n=1$  for the gray level images considered in this work. Let  $C$  be a closed contour in the image domain  $\Omega$ , which separates  $\Omega$  into two regions:  $\Omega_1=outside(C)$  and  $\Omega_2=inside(C)$ . For a given point  $\mathbf{x} \in \Omega$  they define the following local intensity fitting energy:

$$\varepsilon_{\mathbf{x}}^{\text{Fit}}(C, f_1(\mathbf{x}), f_2(\mathbf{x})) = \sum_{i=1}^2 \lambda_i \int_{\Omega_i} K(\mathbf{x}-\mathbf{y}) |I(\mathbf{y}) - f_i(\mathbf{x})|^2 d\mathbf{y} \quad (10)$$

where  $\lambda_1$  and  $\lambda_2$  are positive constants, and  $f_1(\mathbf{x})$  and  $f_2(\mathbf{x})$  are two values that approximate image intensities in  $\Omega_1$  and  $\Omega_2$ , respectively. The intensities  $\mathbf{I}(\mathbf{y})$  that are effectively involved in the above fitting energy are in a local region centered at the point  $\mathbf{x}$ , whose size can be controlled by a kernel function  $K$  [14]. The local intensity fitting energy in (10) is called a *region-scalable fitting* (RSF) energy of a contour  $C$  at a point  $\mathbf{x}$ .

The fitting energy in (3) is region-scalable so that the fitting values  $f_1(\mathbf{x})$  and  $f_2(\mathbf{x})$  approximate the image intensities in a region centered at the point  $\mathbf{x}$ , whose size can be controlled by the scale parameters  $\sigma$  (Gaussian kernel). This region-scalability is a unique and desirable feature of the proposed method. To obtain the entire object boundary, a contour  $C$  must be found that minimizes the energy  $\varepsilon_{\mathbf{x}}^{\text{Fit}}$  for all  $\mathbf{x}$  in the image domain  $\Omega$ . This can be achieved by minimizing the integral over all center points  $\mathbf{x}$ , in the image domain.

In addition, it is necessary to smooth the contour  $C$  by penalizing its length  $|C|$ , as in most of active contour models. Then the following energy functional can be defined for a contour  $C$ ,

$$\mathcal{E}(C, f_1(\mathbf{x}), f_2(\mathbf{x})) = \int \varepsilon_{\mathbf{x}}^{\text{Fit}}(C, f_1(\mathbf{x}), f_2(\mathbf{x})) d\mathbf{x} + \nu |C| \quad (11)$$

Following the level set formulation applied to the piecewise-constant active contour model, the energy functional can be expressed as

$$\mathcal{E}_{\mathbf{x}}^{\text{Fit}}(\phi, f_1(\mathbf{x}), f_2(\mathbf{x})) = \sum_{i=1}^2 \lambda_i \int K_{\sigma}(\mathbf{x}-\mathbf{y}) |I(\mathbf{y}) - f_i(\mathbf{x})|^2 M_i(\phi(\mathbf{y})) d\mathbf{y} \quad (12)$$

where  $M_1(\phi) = H(\phi)$  and  $M_2(\phi) = 1 - H(\phi)$ . Considering, now, the length of the zero level contour, which can be expressed as the integral  $\int |\nabla H(\phi(\mathbf{x}))| d\mathbf{x}$ , the heaviside and delta functions regularized to  $H_{\varepsilon}$  and  $\delta_{\varepsilon}$ , the energy functional  $\varepsilon$  in (12) can be approximated by,

$$\begin{aligned} \mathcal{E}_{\varepsilon}(\phi, f_1(\mathbf{x}), f_2(\mathbf{x})) &= \sum_{i=1}^2 \lambda_i \int \left( \int K_{\sigma}(\mathbf{x}-\mathbf{y}) |I(\mathbf{y}) - f_i(\mathbf{x})|^2 M_i^{\varepsilon}(\phi(\mathbf{y})) d\mathbf{y} \right) d\mathbf{x} \\ &+ \nu \int |\nabla H_{\varepsilon}(\phi(\mathbf{x}))| d\mathbf{x} \end{aligned} \quad (13)$$

To preserve the regularity of the level set function, which is necessary for accurate computation and stable level set evolution, a level set regularization term is added to the variational level set formulation (see [3]). Thus, the energy functional to minimize is

$$F(\phi, f_1, f_2) = \varepsilon_\varepsilon(\phi, f_1, f_2) + \mu P(\phi) \quad (14)$$

Where  $P$  characterizes the deviation of the function from a signed distance function, and  $\mu$  is a positive constant. To minimize this energy functional, its gradient flow is used as the level set evolution equation.

### 2.2.1. Energy Minimization

The standard gradient descent (or steepest descent) method is used to minimize the energy functional (14). By calculus of variations, it can be shown that the functions  $f_1(\mathbf{x})$  and  $f_2(\mathbf{x})$  that minimize  $F(\phi, f_1, f_2)$  satisfy the following Euler–Lagrange equations:

$$\int K_\sigma(\mathbf{x}-\mathbf{y}) |I(\mathbf{y}) - f_i(\mathbf{x})|^2 M_i^\varepsilon(\phi(\mathbf{y})) d\mathbf{y} = 0, \quad i = 1, 2. \quad (15)$$

From Eq. (15),

$$f_i(\mathbf{x}) = \frac{K_\sigma(\mathbf{x}) * [M_i^\varepsilon(\phi(\mathbf{x})) I(\mathbf{x})]}{K_\sigma(\mathbf{x}) * M_i^\varepsilon(\phi(\mathbf{x}))}, \quad i = 1, 2 \quad (16)$$

which minimize the energy functional  $F(\phi, f_1, f_2)$  for a fixed  $\phi$ . The functions  $f_1(\mathbf{x})$  and  $f_2(\mathbf{x})$  given by (16) are weighted averages of the intensities in a neighborhood of  $\mathbf{x}$ , whose size is proportional to the scale parameter  $\sigma$ .

Keeping  $f_1$  and  $f_2$  fixed, we minimize the energy functional  $F(\phi, f_1, f_2)$  with respect to  $\phi$  using the standard gradient descent method by solving the *gradient flow equation* as follows:

$$\begin{aligned} \frac{\partial \phi}{\partial t} = & -\delta_\varepsilon(\phi) (\lambda_1 e_1 - \lambda_2 e_2) + \nu \delta_\varepsilon(\phi) \operatorname{div} \left( \frac{\nabla \phi}{|\nabla \phi|} \right) \\ & + \mu \left( \nabla^2 \phi - \operatorname{div} \left( \frac{\nabla \phi}{|\nabla \phi|} \right) \right) \end{aligned} \quad (17)$$

where

$$e_i(\mathbf{x}) = \int K_\sigma(\mathbf{x}-\mathbf{y}) |I(\mathbf{x}) - f_i(\mathbf{y})|^2 d\mathbf{y}, \quad i = 1, 2 \quad (18)$$

The expression (17) is the level set evolution equation to be solved in the proposed method. The term  $-\delta_\varepsilon(\phi) (\lambda_1 e_1 - \lambda_2 e_2)$  is derived from the data fitting energy and, therefore, is called the *data fitting term*. This term plays a key role in the proposed model, since it is responsible for driving the active contour toward object boundaries.

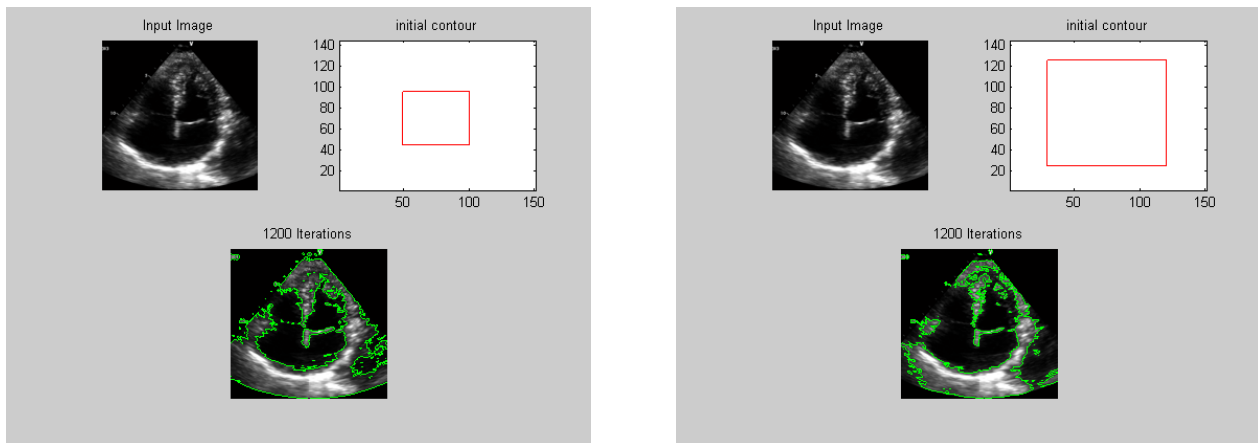
The second term  $\nu \delta_\varepsilon(\phi) \operatorname{div}(\frac{\nabla \phi}{|\nabla \phi|})$  has a smoothing effect on the zero level contour, which is necessary to maintain the regularity of the contour. This term is called the *arc length term*. The third term  $\mu (\nabla^2 \phi - \operatorname{div}(\frac{\nabla \phi}{|\nabla \phi|}))$  is called a *level set regularization term*, since it serves to maintain the regularity of the level set function.

### 3. Experimental results on echocardiographic images

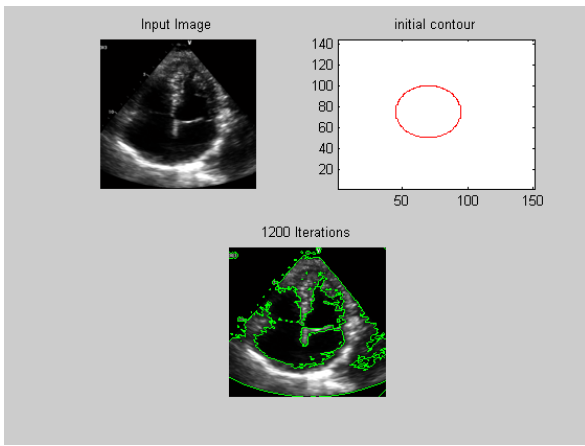
As already mentioned this work aims to compare the quality of the segmentation of the two approaches on real medical images, namely echocardiographic images of newborns. To evaluate the performance, we quantified the robustness of the two different active contour models: computing the position, shape, and propagation direction of the initial contour; convergence time for each algorithm; and image smoothing effect. All images were 640x480 greyscale resized to reduce the computation time.

#### 3.1. Effect of the initial contour shape and size in the active contour evolution

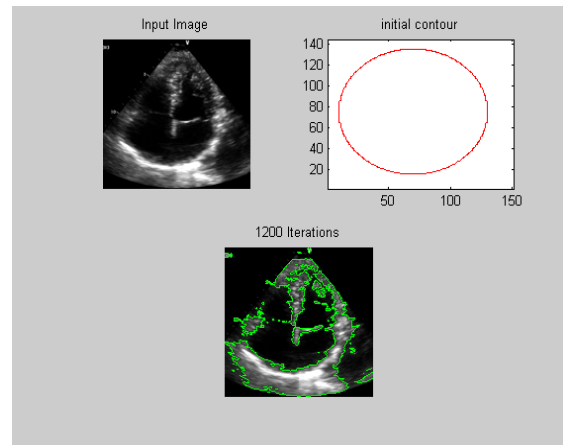
The initialization of the active contour model can be problematic: it must be simple, possibly automatic, and close enough to the objects. First, we analyse the performance of the two approaches to detect boundaries starting with only one initial curve, using images with and without smoothing. For both approaches, two different geometric initial contours were used: rectangular and circular. Figures 1a and 1b illustrate the rectangular initial contour applied in the Chan and Vese model for echocardiographic image segmentation of newborns: inside and outside the ROI (Region-Of-Interest), respectively. It was processed 1200 iterations for all experimental situations and for the Chan model, the following parameter values were used:  $\mu = 0.2$ ;  $\lambda_1=1$ ,  $\lambda_2=1$  and  $\nu=0$ . It seems that the internal initialization could perform better, however it needs additional iterations to reach the same degree of segmentation provided by external contour. Computational time was similar for both initializations. Figures 2a and 2b show the segmentation results for a circular initial contour using the same parameters and iterations. From previous figures, it is apparent a segmentation improvement with circular initialization compared to the rectangular one, especially with the external contour where the boundaries are better defined. Nevertheless, this circular external initial contour needs more time to adapt to the boundaries for the same iterations. We also applied the Chunming Li model to the same echocardiographic images to evaluate the performance of the two approaches. The parameters selected for the processing were:  $\mu = 1$ ,  $\lambda_1=2$ ,  $\lambda_2 = 3$ ,  $\epsilon=1$ ,  $\sigma = 1$ , and timestep=0.1.



(a) (b)  
Fig. 1. Active contour proposed by Chan and Vese with rectangular initial contour;  
(a) initial contour inside the ROI and (b) external to the ROI.



(a)



(b)

Fig. 2. Active contour proposed by Chan and Vese with circular initial contour; (a) initial contour inside the ROI and (b) external to the ROI.

An important observation can be taken about the time performance of the two models: the variational level set proposed by Li is faster than the one by Chan, as can be seen in figure 3(a), where only 200 iterations were enough to reach the same level of segmentation. Additional iterations and some changing of parameters did not improve the contours. As the size of initial contour increases the algorithm needs much more time to converge.

Thus, we can mention, as an important advantage, the fact that the initial curves (rectangular or circular) evolve quite well to the boundaries in the Chan model, independent of the contours size. Also, it is insensitive to the location of the initial contour related to the ROI of the echocardiographic images. The Li model is faster but presents some limitations concerning to initialization.

### 3.2. Effect of the initial contour position in the active contour evolution

Another experimental work dealt with the behaviour of the active contour evolution when initial contour was placed completely outside the object to segment. The computing using the Li model demonstrates that curve evolution is insensitive to the position of the initial contour and this has no influence in the convergence of the model, as illustrated in figure 4. For comparison, the same simulation was made for the Chan model and the curve evolves to the boundaries very slowly; even for 2000 iterations, the segmentation is not completed as shown in figure 5.

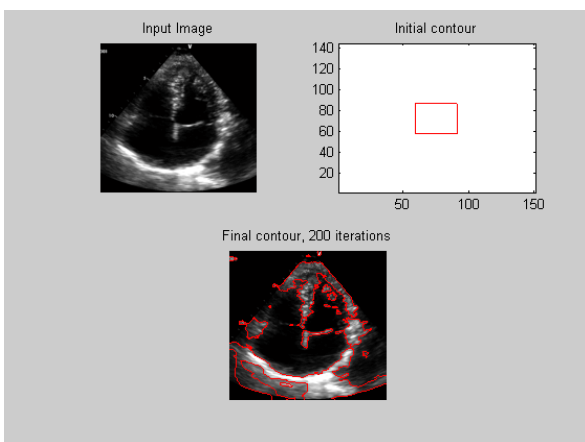


Fig. 3. Active contour proposed by Chunming Li. Initial contour inside the ROI

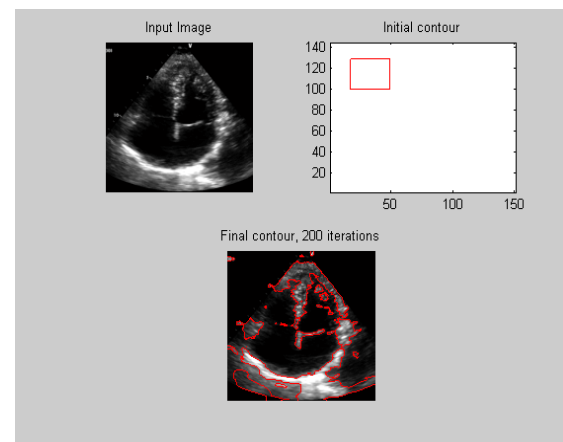


Fig. 4. Active contour proposed by Chunming Li. Behaviour *versus* position of initial contour

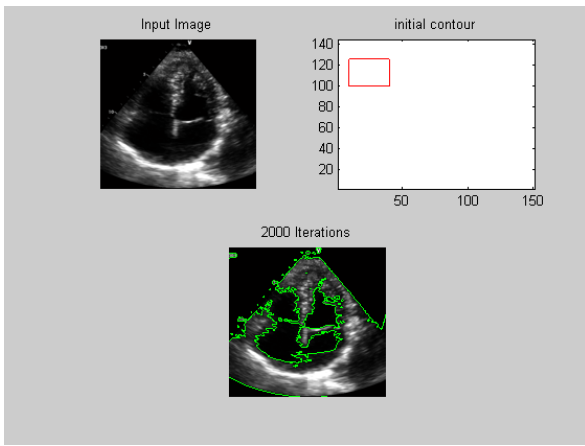


Fig.5. Active contour proposed by Chan and Vese.  
Behaviour *versus* position of initial contour

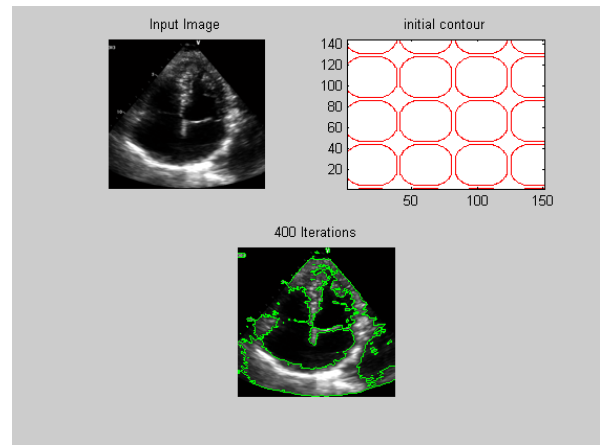
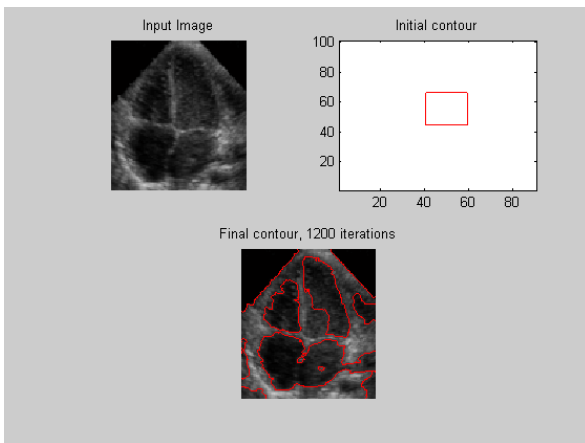


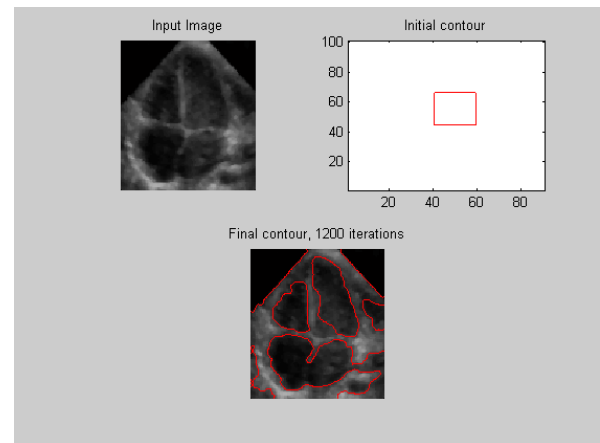
Fig.6. Active contour proposed by Chan and Vese  
Behaviour *versus* multiple initial contours

Segmentation is of great importance for 3D reconstruction of organs and to aid physicians to visualize and diagnosis diseases. These goals are only effective if made on reasonable time. So, to perform the segmentation and to achieve the previous goals, it is necessary an automatic initialization of the active contour, which could not be easy. A simply way to increase the speed of the segmentation process consists of using several initial contour filling the whole image. As it is demonstrated in figure 6 that procedure leads to segmentation result similar to the one using only one initial contour, however with a clear advantage in terms of convergence time.

The methods were also applied in noisy images. Figure 7(a) illustrates an image collected by a cardiac 6MHz probe were it is clear a lower contrast between boundaries and cavities. Also, it can be seen that the contour does not adjust to the boundaries in spite of their robustness to the presence of weak boundaries and noise. Attenuating the noise using a median filter, which is a nonlinear operation often used in image processing to reduce "salt and pepper" noise, did not produce better results as shown in figure 7(b). However, the Li model presents higher robustness for these kind of images.



(a)



(b)

Fig.7 - Active contour proposed by Chunming Li. (a) Echocardiographic image with a high resolution probe (6 MHz); (b) The same image with median filtering ([3 3]).

#### 4. Conclusions

In this work, we present a comparative study about the segmentation ability of two implicit deformable models applied to echocardiographic images of newborns. Parameters like, shape and size of initial contours, position in the images and propagation direction of the level set were tested.

It was observed that both models are relatively less sensible to the size and position of the initial contour in the image. The observed differences are related to the convergence time that is considerable higher for the Chan model. The propagation direction of the level set has no relevancy in the two models. Also, if the initialization is completely outside the ROI, the Chan model needs much more time to adjust the contour to the boundaries. It should be pointed out that both algorithms are very slow whether 3D reconstruction is the final goal. A simply way to increase the speed of the segmentation process consists of using several initial contour filling the whole image. As demonstrated, that leads to low convergence time and reduce completely the uncertainty about the best initialization in an automatic segmentation. Smoothed images by median filter have not given rise to fast convergence. As a final conclusion we can say that the models are adaptable to the tested images, producing satisfactory results.

## References

- [1] Caselles V, Kimmel R, Shapiro G. Geodesic active contours. *Int J Comput Vis* 1997; 22, 61–79.
- [2] Malladi R, Sethian JA, Vemuri BC. Shape modeling with front propagation. *IEEE Trans Pattern Anal Mach Intell* 1995;17(2):158–75.
- [3] Cohen L. On active contour models and balloons. *Computer vision, graphics, and image processing. Image Understanding* 1991;53(2):211–8.
- [4] Cohen L, Cohen I. Finite-element methods for active contour models and balloons for 2-d and 3-d images. *IEEE Trans Pattern Anal Mach Intell* 1993;15(11):1131–46.
- [5] Chan TF, Vese LA. Active contours without edges. *IEEE Trans Image Process* 2001; 10(2):266–77.
- [6] Zhu SC, Yuille A. Region competition: unifying snakes, region grouping, and Bayes/MDL for multiband image segmentation. *IEEE Trans Pattern Anal Mach Intell* 1996;18(9):884–900.
- [7] Mumford D, Shah J. Optimal approximation by piecewise smooth functions and associated variational problems. *Communication Pure Appl Math* 1989;42(5):577–685.
- [8] Frederic P, Michel B, Thierry B, et al. Robust real-time segmentation of images and videos using a smooth-spline snake-based algorithm. *IEEE Trans Image Process* 2005;14(7):910–24.
- [9] Mukherjee DP, Ray N, Acton ST. Level set analysis for leukocyte detection and tracking. *IEEE Trans Image Process* 2004; 13(4):562–72.
- [10] Freedman D, Zhang T. Active contours for tracking distributions. *IEEE Trans Image Process* 2004; 13(4):518–26.
- [11] V. Caselles, R. Kimmel, and G. Sapiro, “Geodesic active contours,” *International Journal of Computer Vision*, 1997, no. 1, pp. 61–79.
- [12] V. Caselles, R. Kimmel, and G. Sapiro, “Geodesic active contours,” in *Proc. of IEEE International Conference on Computer Vision*, 1995, p. 694.
- [13] V. Caselles, F. Catte, T. Coll, and F. Dibos, “A geometric model for active contours,” *Numerische Mathematik*, 1993, p. 19.
- [14] M. Kass, A. Witkin, and D. Terzopoulos. Snakes: Active contour models. *International Journal of Computer Vision*, 1988,1:321–331.
- [15] D. Mumford and J. Shah, “Boundary detection by minimizing functionals,” in *Proc. of IEEE Conference on Computer Vision and Pattern Recognition*, 1985.
- [16]. Chunming Li, Chiu-Yen Kao, John C. Gore, and Zhaohua Ding, Minimization of Region-Scalable Fitting Energy for Image Segmentation. *IEEE Transactions on image processing*, 2008, vol. 17, no. 10 .
- [17] Osher, S., Sethian, J. A., *Fronts Propagating with Curvature-Dependent Speed: Algorithms Based on Hamilton-Jacobi Formulation. Journal of Computational Physics*, 1988, 79, 12-49.